BIOCHEMISTRY
including biophysical chemistry & molecular biology

Article

pubs.acs.org/biochemistry

Reduction Kinetics of 3-Hydroxybenzoate 6-Hydroxylase from *Rhodococcus jostii* RHA1

Jeerus Sucharitakul,*[,†] Thanyaporn Wongnate,[‡] Stefania Montersino,[§] Willem J. H. van Berkel,[§] and Pimchai Chaiyen[‡]

[†]Department of Biochemistry, Faculty of Dentistry, Chulalongkorn University, Henri Dunant Road, Patumwan, Bangkok 10330, Thailand

[‡]Department of Biochemistry and Center of Excellence in Protein Structure and Function, Faculty of Science, Mahidol University, Rama VI Road, Bangkok 10400, Thailand

[§]Laboratory of Biochemistry, Wageningen University, Dreijenlaan 3, 6703 HA Wageningen, The Netherlands

ABSTRACT: 3-Hydroxybenzoate 6-hydroxylase (3HB6H) from *Rhodococcus jostii* RHA1 is a nicotinamide adenine dinucleotide (NADH)-specific flavoprotein monooxygenase involved in microbial aromatic degradation. The enzyme catalyzes the para hydroxylation of 3-hydroxybenzoate (3-HB) to 2,5-dihydroxybenzoate (2,5-DHB), the ring-fission fuel of the gentisate pathway. In this study, the kinetics of reduction of the enzyme-bound flavin by NADH was investigated at pH 8.0 using a stopped-flow spectrophotometer, and the data were analyzed comprehensively according to kinetic derivations and simulations. Observed rate constants for reduction of the free enzyme by NADH under anaerobic conditions were linearly dependent on NADH concentrations, consistent with a one-step irreversible reduction model with a bimolecular rate constant of 43 ± 2 M^{-1} s^{-1}. In the presence of 3-HB, observed rate constants for flavin reduction were hyperbolically dependent on NADH concentrations and approached a limiting value of 48 ± 2 s^{-1}. At saturating concentrations of NADH (10 mM) and 3-HB (10 mM), the reduction rate constant is ~51 s^{-1}, whereas without 3-HB, the rate constant is 0.43 s^{-1} at a similar NADH concentration. A similar stimulation of flavin reduction was found for the enzyme−product (2,5-DHB) complex, with a rate constant of 45 ± 2 s^{-1}. The rate enhancement induced by aromatic ligands is not due to a thermodynamic driving force because E^0_m for the enzyme−substrate complex is −179 ± 1 mV compared to an E^0_m of −175 ± 2 mV for the free enzyme. It is proposed that the reduction mechanism of 3HB6H involves an isomerization of the initial enzyme−ligand complex to a fully activated form before flavin reduction takes place.

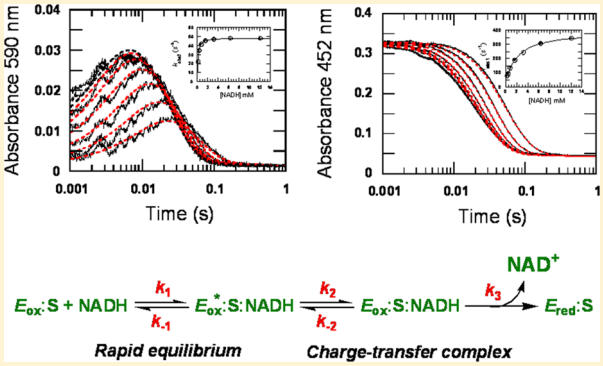

Phenolic compounds are among the major chemical constituents in the biosphere. These compounds originate from natural sources such as decaying lignin (a complex phenolic polymer in plant) or from industrial activity.[1] Accumulation of phenolic compounds from man-made chemicals causes environmental pollution, as the aromatic compounds are difficult to degrade.[2] Therefore, aerobic degradation of natural and xenobiotic aromatic compounds by microorganisms is useful in bioremediation as it provides environmental friendly means of converting phenolic species to nontoxic compounds.[3] Gram-negative bacteria such as *Pseudomonas*, *Sphingomonas*, *Acinetobacter*, *Ralstonia*, and *Burkholderia*[1,4] are known for possessing a variety of monooxygenases involved in aromatic degradation. These enzymes convert phenolic compounds to the corresponding dihydroxybenzenes, which can be further degraded to intermediates of the citric acid cycle.[5] The genus *Rhodococcus* is regarded as one of the most promising Gram-positive microorganisms that is suitable for the bioremediation process of toxic xenobiotics[6] because its cell wall contains hydrophobic mycolic acids, which could facilitate the uptake of hydrophobic substrates.[7,8] In addition, its ability to modulate the fatty acid composition of membrane lipids can alter cell envelope fluidity, which allows the cell to be resistant to many toxic compounds.[8]

Until now, only a few phenolic monooxygenases from *Rhodococcus* sp. have been studied.[9,10] Recently, a novel monooxygenase from *Rhodococcus jostii* RHA1 catalyzing the para hydroxylation of 3-hydroxybenzoate (3-HB) was cloned, expressed, and biochemically characterized.[11] 3-Hydroxybenzoate 6-hydroxylase (3HB6H) from *R. jostii* RHA1 is a nicotinamide adenine dinucleotide (NADH)-specific flavoprotein that catalyzes the hydroxylation of 3-HB at C6 to form 2,5-dihydroxybenzoate (2,5-DHB) as a product (Scheme 1). The enzyme is a homodimer and contains one FAD per subunit of 47 kDa.[11]

Received: December 10, 2011
Revised: May 2, 2012
Published: May 4, 2012

Scheme 1. Catalytic Reaction of 3HB6H

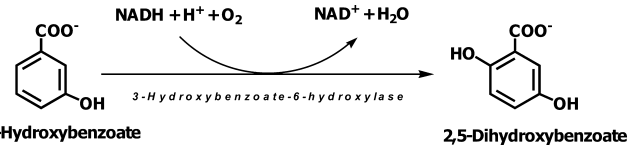

3HB6H belongs to subclass A of the flavoprotein monooxygenases that utilize single polypeptides to catalyze hydroxylation reactions.[11,12] On the basis of sequence similarity, 3HB6H is closely related to *p*-hydroxybenzoate hydroxylase (PHBH)[13−15] or 2-methyl-3-hydroxypyridine carboxylic acid oxygenase (MHPCO).[16] Like those of other single-component flavoprotein hydroxylases, the catalytic reaction of 3HB6H consists of two half-reactions.[15,17] The first half-reaction of these enzymes is the reduction of an FAD cofactor by the external reductant NAD(P)H, while the second half-reaction is the reaction of the reduced enzyme with molecular oxygen to form a reactive intermediate that is capable of hydroxylating phenolic compounds.[12,18] The genes encoding this enzyme in other microorganisms have also been identified,[19−23] but catalytic properties have not been investigated except for the enzymes from *Pseudomonas cepacia*[24] and *Micrococcus* sp.[25] in which their steady-state kinetics parameters have been reported.[26] Currently, it is not known if 3HB6H, which is unique for hydroxylation at the para position, utilizes a kinetic mechanism similar to that of the related ortho hydroxylases.

In this study, we have investigated the transient kinetics of the reductive half-reaction of 3HB6H in the presence and absence of the aromatic substrate (3-HB) and product (2,5-DHB). The results demonstrate the effector function of these aromatic compounds and highlight different catalytic properties of 3HB6H compared to those of other family members.

EXPERIMENTAL PROCEDURES

Reagents. NADH (≥94% pure), FAD (≥95% pure), D-glucose (99.5% pure), and catalase were purchased from Sigma-Aldrich. 3-HB and 2,5-DHB were purchased from Merck. Concentrations of the following compounds were determined using the known absorption coefficient values: for NADH, ε_{340} = 6.22 mM^{-1} cm^{-1}; for FAD, ε_{450} = 11.3 mM^{-1} cm^{-1}; for 3-HB, ε_{288} = 2.0 mM^{-1} cm^{-1}; for 2,5-DHB, ε_{320} = 4.1 mM^{-1} cm^{-1}. All the extinction coefficient values were obtained at pH 8.0.

Enzyme Preparation. The gene of 3HB6H was cloned into the pBAD/Myc-His vector, which contains an N-terminal His_6 tag and an ampicillin resistance gene and was expressed in *Escherichia coli* (TOP10).[11] A single colony of freshly grown *E. coli* was inoculated into 100 mL of terrific broth medium (in a 500 mL Erlenmeyer flask), containing 100 μg/mL ampicillin, and incubated overnight in an orbital shaker at 37 °C. An overnight culture (5 mL) was inoculated into 6 × 800 mL of terrific broth containing 50 μg/mL ampicillin. The large-scale cell culture was incubated in an orbital shaker at 37 °C until the absorbance at 600 nm reached ∼2 (∼3 h). Overexpression of the enzyme was induced via addition of 0.02% L-arabinose to the culture. The culture was allowed to grow at 37 °C for an additional 7 h and then harvested. The yield of cell paste was typically ∼64 g per 4.8 L of cell culture.

Enzyme Purification. Because of the availability of conventional chromatographic media in our laboratory, enzyme purification was conducted using DEAE-Sepharose, which resulted in an efficient purification process. Cell lysis was conducted in 100 mM sodium phosphate (pH 7.0) containing 65 μM phenylmethanesulfonyl fluoride (PMSF), 1 mM dithiothreitol (DTT), and 1 mM EDTA using a 750 W ultrasonic processor Vibra cell model. The temperature during the cell lysis process was kept below 10 °C using an ice bath. The resulting sonicated suspension was centrifuged at 13700*g* for 30 min at 4 °C, and the supernatant was collected. Nucleic acid materials were removed by adding a solution of 0.1% polyethyleneimine (10 mL). The resulting suspension was centrifuged at 13700*g* for 20 min to separate the pellet and clear supernatant. The pellet was discarded, and the supernatant was brought to 35% ammonium sulfate saturation (20.8 g/100 mL). After centrifugation at 13700*g* for 20 min, the resulting supernatant was brought to 80% ammonium sulfate saturation (31.6 g/100 mL). The resulting yellow pellet was resuspended in 50 mM sodium phosphate (pH 7.0) containing 0.5 mM EDTA, and the solution was dialyzed in 4 L of the same buffer for 18 h. The dialyzed enzyme solution was loaded onto a DEAE-Sepharose column (ϕ 2.5 cm × 38 cm) pre-equilibrated with 50 mM sodium phosphate (pH 7.0) containing 150 mM NaCl and 0.5 mM EDTA. 3HB6H eluted with a gradient from 150 to 350 mM NaCl in 50 mM sodium phosphate buffer (pH 7.0) and 0.5 mM EDTA. Fractions containing 3HB6H were identified by absorbance at 452 nm, pooled, and concentrated using a stirred cell device (Amicon) with a molecular mass cutoff of 10 kDa to obtain a solution volume of ∼6−8 mL. Free FAD was added during the enzyme concentrating process to make sure that the enzyme was fully bound to FAD. The concentrated enzyme was passed through a Sephadex G-25 gel filtration column (ϕ 1.5 cm × 40 cm) pre-equilibrated with 100 mM MOPS (morpholinopropane sulfonic acid) (pH 7.0). The purity of the enzyme was greater than 98% as judged by sodium dodecyl sulfate−polyacrylamide gel electrophoresis. A typical yield of the preparation process is ∼50 mg/L of cell culture. The enzyme solution was aliquoted into microcentrifuge tubes (500 μL each) and kept at −80 °C. Before being used, the enzyme solution was quickly thawed and exchanged into 50 mM Tris-H_2SO_4 (pH 8.0) using a PD-10 column (GE Healthcare).

Spectroscopic Studies. UV−visible absorbance spectra were recorded using a Hewlett-Packard diode array spectrophotometer (HP8453), a Shimadzu 2501PC spectrophotometer, or a Cary 300Bio split-beam spectrophotometer. All spectrophotometers were equipped with thermostated cell compartments. The enzyme assay reaction mixture consisted of 10 mM 3HB, 1 mM NADH, and 20 μM FAD. Enzyme activities were determined by a continuous assay based on a decrease in absorbance at 340 nm (for NADH, ε_{340} = 6.22 mM^{-1} cm^{-1}) because of NADH oxidation.

Molar Absorption Coefficient of Enzyme-Bound FAD. A solution of the holoenzyme was diluted in 50 mM Tris-H_2SO_4 (pH 8.0) to obtain the absorbance at 452 nm of ∼0.3. The holoenzyme solution (900 μL) was added to a solution of 2% SDS (100 μL) to obtain a final SDS concentration of 0.2%. The concentration of free FAD released from the denatured enzyme was determined on the basis of a molar absorption coefficient for free FAD (ε_{450}) of 11.3 mM^{-1} cm^{-1}. After correcting for the dilution effect, we calculated the molar absorption coefficient of the enzyme (per FAD molecule) (ε_{452}) to be 11.00 ± 0.03 mM^{-1} cm^{-1}.

Dissociation Constants of Enzyme−Ligand Complexes. Binding experiments were conducted in 50 mM Tris-

dx.doi.org/10.1021/bi201823c | *Biochemistry* 2012, 51, 4309−4321

H_2SO_4 (pH 8.0) at 25 °C. Perturbation of the 3HB6H flavin absorption spectrum due to substrate binding was measured using a split-beam spectrophotometer to record difference spectra. Two cuvettes containing a solution of 27 μM enzyme were placed in both sample and reference cells. Equal volumes of the substrate and the buffer solution were added to the sample and reference cuvette, respectively. Absorbance changes at 491 nm were plotted against the free substrate concentration to obtain the dissociation constant (K_d). The K_d was analyzed according to the eq 1 using Marquardt−Levenberg nonlinear fitting algorithms included in KaleidaGraph (Synergy Software). Similar analysis was applied for the determination of the K_d of the enzyme−2,5-DHB complex.

$$[ES] = [[E_T] + [L_T] + K_d - \sqrt{([E_T] + [L_T] + K_d)^2 - 4[E_T][L_T]}]/2 \quad (1)$$

where [ES] is the concentration of the enzyme−ligand complex at a given ligand concentration, $[E_T]$ is the total enzyme concentration, and $[L_T]$ is the total ligand concentration.

Rapid Reaction Experiments. Reactions were conducted in 50 mM Tris-H_2SO_4 (pH 8.0) at 4 °C, unless otherwise specified. The measurements were performed using a TgK Scientific model SF-61DX or TgK Scientific model SHU-61SX2 stopped-flow spectrophotometer in single-mixing mode. The optical path length of the observation cell was 1 cm. The stopped-flow instrument was made anaerobic by flushing the flow system with an anaerobic buffer solution containing 400 μM D-glucose, 100 μg/mL glucose oxidase, and 4.8 μg/mL catalase in 50 mM sodium phosphate (pH 7.0). The buffer used for the glucose/glucose oxidase system was equilibrated in an anaerobic glovebox (Belle Technology) for 18 h (overnight) to remove oxygen. D-Glucose, glucose oxidase, and catalase were added to the anaerobic buffer inside the glovebox. The resulting glucose/glucose oxidase solution was transferred into tonometers, put onto the stopped-flow system, and allowed to stand in the flow system overnight. The flow unit was then rinsed with an anaerobic buffer before the experiments were conducted.

For studying the kinetics and thermodynamics of substrate binding, a solution of oxidized enzyme in 50 mM Tris-H_2SO_4 (pH 8.0) was mixed with solutions of the same buffer containing various concentrations of 3-HB using a stopped-flow instrument. All concentrations of 3-HB used for rapid kinetics studies were at least 6.5-fold higher than the enzyme concentration used to maintain pseudo-first-order conditions. Simulations were performed by numerical methods using Runge−Kutta algorithms implemented in Berkeley Madonna 8.3 and a time step of 1×10^{-4} s. Simulations according to the model proposed were conducted, and the results were compared with the stopped-flow data.

For studying the kinetics of reduction of the enzyme by NADH, a solution of oxidized 3HB6H with or without 3-HB (or 2,5-DHB) was placed in a tonometer equilibrated with oxygen-free nitrogen and then loaded onto the stopped-flow machine. The oxygen-free nitrogen gas (ultrahigh purity) used for equilibration was passed through an Oxyclear oxygen removal column (Labclear). NADH solutions (3 mL) at various concentrations in 50 mM Tris-H_2SO_4 (pH 8.0) were placed in a 5 mL glass syringe and made anaerobic by bubbling with oxygen-free nitrogen for 8 min before being loaded onto the stopped-flow instrument. All concentrations of NADH used for rapid kinetic studies were at least 7-fold higher than the enzyme concentration used to maintain pseudo-first-order conditions.

Observed reduction rate constants (k_{obs}) were calculated from kinetic traces using exponential fits and the software package in Kinetic Studio 1.08 (TgK Scientific, Bradford-on-Avon, U.K.) and Program A [written at the University of Michigan (Ann Arbor, MI) by R. Chang, J.-y. Chiu, J. Dinverno, and D. P. Ballou]. Rate constants were obtained from fits of k_{obs} versus NADH concentration using Marquardt−Levenberg nonlinear fitting algorithms included in KaleidaGraph (Synergy Software). Simulations were performed by numerical methods using Runge−Kutta algorithms implemented in Berkeley Madonna 8.3 and a time step of 7.8125×10^{-6} s for simulations of the reductive half-reaction of the enzyme−3-HB complex and a time step of 2×10^{-4} s for simulations of the reductive half-reaction of the enzyme−2,5-DHB complex. The kinetic model used for these simulations is described below.

Determination of Standard Reduction Potential Values. Reduction potential values of 3HB6H, in the presence and absence of 3-HB, in 50 mM Tris-H_2SO_4 (pH 8.0) at 25 °C were measured by Massey's method.[27] Xanthine (0.5 mM) and xanthine oxidase (10 nM) were used to catalytically reduce the enzyme. Benzyl viologen (5 μM) was used as an electron mediator. The enzyme and dye were slowly reduced to reach equilibrium (~8 h for complete reduction). The reduction potentials of the enzyme (E_{red}) and dye (D_{ox}) are determined according to eqs 2 and 3:

$$E_e = E_e^0 - \frac{0.0592}{n_e} \log(E_{red}/E_{ox}) \quad (2)$$

$$E_d = E_d^0 - \frac{0.0592}{n_d} \log(D_{red}/D_{ox}) \quad (3)$$

The reference dye employed for the determination of redox potentials for both the free enzyme and the enzyme−3-HB complex was indigo disulfonate ($E_m^0 = -116$ mV at pH 7.0).[28] According to the equation $\Delta E_m/\Delta pH = -0.06$ V,[29] the E_m^0 value at pH 8.0 was calculated as −176 mV. The absorbances at 458 nm (isosbestic point of dye) and 610 nm were used to calculate the concentrations of oxidized enzyme (E_{ox}) and dye (D_{red}) during the reduction process, respectively. These data were then used to calculate the corresponding concentrations of the reduced enzyme (E_{red}) and oxidized dye (D_{ox}) for plotting $\log(E_{red}/E_{ox})$ on the y-axis and $\log(D_{red}/D_{ox})$ on the x-axis. The standard redox potential value of the enzyme (E_e^0) was calculated from the y-intercept of the plot according to eq 4. At equilibrium, the value of E_e is equivalent to E_d and eqs 2 and 3 can be rearranged as

$$\log(E_{red}/E_{ox}) = \frac{n_e(E_e^0 - E_d^0)}{0.0592} + (n_e/n_d) \log(D_{red}/D_{ox}) \quad (4)$$

Relationship of Observed and Individual Rate Constants. A kinetic model for the NADH-dependent reduction of protein-bound flavin is shown in Scheme 2.

Scheme 2. Three-Step Equilibrium Reaction

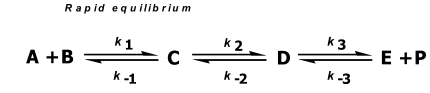

dx.doi.org/10.1021/bi201823c | Biochemistry 2012, 51, 4309−4321

According to the model used in this report, the first bimolecular reaction is assumed to be a rapid equilibrium process in which the relaxation time is considerably shorter than those of the second and third steps whereas the relaxation times of the second and third steps are comparable ($k_1 + k_{-1} \gg k_2 + k_{-2}$, $k_3 + k_{-3}$).

$$c_A = \bar{c}_A + \Delta c_A$$

$$c_B = \bar{c}_B + \Delta c_B$$

$$c_C = \bar{c}_C + \Delta c_C$$

$$c_D = \bar{c}_D + \Delta c_D$$

$$c_E = \bar{c}_E + \Delta c_E$$

where c_i (i = A, B, C, D, or E) is a concentration at any given time (t), $\bar{c}_i$ is a concentration at equilibrium, and Δc_i is defined as $c_i - \bar{c}_i$ (the change in concentration with reference to the final equilibrium concentration at any given time). The method used for the derivations herein was modified from that of Bernasconi.[30]

To define the relaxation time of the second and third steps, the first step is assumed to be at equilibrium ($1 \leftrightarrow 2$) while the second and third steps are relaxing. Although equilibration of the first step does not lead to the establishment of the final equilibrium concentrations of $\bar{c}_A$, $\bar{c}_B$, $\bar{c}_C$, $\bar{c}_D$, and $\bar{c}_E$, concentrations c_A, c_B, and c_C can be assumed to be pseudoequilibrium concentrations because of the rapid equilibrium of the first step.[30]

Equilibrium constants for A−C in the first step, while the second and third steps are relaxing, can be written according to eq 5:

$$K_1 = \frac{c_C}{c_A c_B} \tag{5}$$

Substitution of $c_A = \bar{c}_A + \Delta c_A$, $c_B = \bar{c}_B + \Delta c_B$, and $c_C = \bar{c}_C + \Delta c_C$ into eq 5 yields eq 6:

$$K_1 = \frac{\bar{c}_C + \Delta c_C}{(\bar{c}_A + \Delta c_A)(\bar{c}_B + \Delta c_B)}, \quad \Delta c_A = \Delta c_B \tag{6}$$

Rearrangement of eq 6 yields eqs 7 and 8:

$$K_1[\bar{c}_A \bar{c}_B + \Delta c_A(\bar{c}_A + \bar{c}_B) + \Delta c_A{}^2] = \bar{c}_C + \Delta c_C \tag{7}$$

$$K_1 \bar{c}_A \bar{c}_B + K_1 \Delta c_A(\bar{c}_A + \bar{c}_B) + K_1 \Delta c_A{}^2 = \bar{c}_C + \Delta c_C \tag{8}$$

For small displacements, $K_1 \Delta c_A{}^2 \approx 0$[30] and $K_1 \bar{c}_A \bar{c}_B = \bar{c}_C$, and rearrangement of eq 8 yields eq 9:

$$K_1 = \frac{\Delta c_C}{(\bar{c}_A + \bar{c}_B)\Delta c_A} \tag{9}$$

Under pseudo-first-order conditions, as $\bar{c}_B \gg \bar{c}_A$, eq 9 can be arranged as eq 10:

$$K_1 = \frac{\Delta c_C}{\Delta c_A[B]} \tag{10}$$

The relationships of observed rate constants for the second step (k_{obs2}) and third step (k_{obs3}) of the rate equations for species D and E were derived according to the rate equation for the law of mass action as written in eqs 11 and 12:

$$\frac{d\Delta c_D}{dt} = k_2 \Delta c_C - (k_{-2} + k_3)\Delta c_D + k_{-3} \Delta c_E[P] \tag{11}$$

$$\frac{d\Delta c_E}{dt} = k_3 \Delta c_D - k_{-3} \Delta c_E[P] \tag{12}$$

According to mass balance, a decrease in the concentration of A (Δc_A) corresponds to an increase in Δc_C, Δc_D, and Δc_E as in eq 13:

$$-\Delta c_A = \Delta c_C + \Delta c_D + \Delta c_E \tag{13}$$

Substitution of Δc_A as described in eq 13 into eq 10 results in eqs 14 and 15:

$$K_1 = -\frac{\Delta c_C}{(\Delta c_C + \Delta c_D + \Delta c_E)[B]} \tag{14}$$

$$\Delta c_C = -\frac{K_1[B](\Delta c_D + \Delta c_E)}{1 + K_1[B]} \tag{15}$$

Substitution of Δc_C (according to eq 15) and $k'_{-3} = k_{-3}[P]$ into eqs 11 and 12 results in eqs 16 and 17:

$$\frac{d\Delta c_D}{dt} + \left(\frac{k_2 K_1[B]}{1 + K_1[B]} + k_{-2} + k_3\right)\Delta c_D + \left(\frac{k_2 K_1[B]}{1 + K_1[B]} - k'_{-3}\right)\Delta c_E = 0 \tag{16}$$

$$\frac{d\Delta c_E}{dt} - k_3 \Delta c_D + k'_{-3} \Delta c_E = 0 \tag{17}$$

Both eqs 16 and 17 are linear homogeneous first-order differential equations according to the form of eq 18:

$$dx_1/dt + a_{11}x_1 + a_{12}x_2 = 0$$

$$dx_2/dt + a_{21}x_1 + a_{22}x_2 = 0 \tag{18}$$

The two differential equations and the reciprocals of the two comparable relaxation times (observed rate constants of the second and third steps in Scheme 2) can be written as in eq 19:[30]

$$(a_{11} - 1/\tau)x_1 + a_{12}x_2 = 0$$

$$a_{12}x_1 + (a_{22} - 1/\tau)x_2 = 0 \tag{19}$$

The determinants of eq 19 can be written as eq 20:

$$\begin{vmatrix} a_{11} - 1/\tau & a_{12} \\ a_{21} & a_{22} - 1/\tau \end{vmatrix} = 0 \tag{20}$$

In analogy to eqs 18−20, eqs 16 and 17 can be written in square matrix format as

$$\begin{vmatrix} \left(\frac{k_2 K_1[B]}{1 + K_1[B]} + k_{-2} + k_3\right) - 1/\tau & \frac{k_2 K_1[B]}{1 + K_1[B]} - k'_{-3} \\ -k_3 & k'_{-3} - 1/\tau \end{vmatrix} = 0 \tag{21}$$

The determinant of the square matrix in eq 21 can be written as the quadratic equation in the form of $ax^2 + bx + c = 0$:

$$(1/\tau)^2 - (a_{11} + a_{22})(1/\tau) + a_{11}a_{22} - a_{12}a_{21} = 0 \tag{22}$$

where

dx.doi.org/10.1021/bi201823c | Biochemistry 2012, 51, 4309−4321

$$a_{11} = \frac{k_2K_1[B]}{1 + K_1[B]} + k_{-2} + k_3 \; a_{12} = \frac{k_2K_1[B]}{1 + K_1[B]} - k'_{-3}$$

$$a_{21} = -k_3 \; a_{22} = k'_{-3}$$

Therefore

$$k_{obs2} = 1/\tau_1 = \frac{-b + \sqrt{b^2 - 4ac}}{2a} \quad (23)$$

$$k_{obs3} = 1/\tau_2 = \frac{-b - \sqrt{b^2 - 4ac}}{2a} \quad (24)$$

where

$$a = 1, \; b = a_{11} + a_{22}, \; c = a_{11}a_{22} - a_{12}a_{21}$$

If $k_{obs2} > k_{obs3}$, substitution of a, b, and c with a_{11}, a_{12}, a_{21}, and a_{22} in eqs 23 and 24, based on the assumption that the last step is irreversible (k_{-3} and $k'_{-3} = 0$) and $K_d = 1/K_1$, results in the relationships of k_{obs2} and k_{obs3} as shown in eqs 25 and 26, respectively:

$$k_{obs2} = \frac{1}{2}\left(\frac{k_2[B]}{K_d + [B]} + k_{-2} + k_3\right) + \left[\frac{1}{4}\left(\frac{k_2[B]}{K_d + [B]} + k_{-2} + k_3\right)^2 - \frac{k_2k_3[B]}{K_d + [B]}\right]^{1/2} \quad (25)$$

$$k_{obs3} = \frac{1}{2}\left(\frac{k_2[B]}{K_d + [B]} + k_{-2} + k_3\right) - \left[\frac{1}{4}\left(\frac{k_2[B]}{K_d + [B]} + k_{-2} + k_3\right)^2 - \frac{k_2k_3[B]}{K_d + [B]}\right]^{1/2} \quad (26)$$

RESULTS

Kinetics of Binding of the Substrate to Oxidized 3HB6H. A solution of the oxidized enzyme (31 μM after mixing) was mixed with various concentrations of 3-HB using a stopped-flow spectrophotometer. The reaction was monitored by the decrease in absorbance at 491 nm, which reflects the spectral perturbation of the oxidized enzyme due to substrate binding. The solid lines (Figure 1) show kinetic traces at various 3-HB concentrations. The results showed that the binding of the substrate to the oxidized enzyme is very fast as a significant part of the absorbance change occurred during the dead time of the stopped-flow mixing even at the lowest concentration of 3-HB employed (Figure 1). A plot of rate constants (k_{obs}) derived from the kinetic traces (○) shows a linear dependence on 3-HB concentration in range of 0.2−1 mM (inset of Figure 1). Therefore, the mechanism for binding of 3-HB to 3HB6H was interpreted as one-step binding (eq 27) of 3-HB to 3HB6H (Scheme 3). However, we cannot absolutely rule out the possibility that the binding may involve extra steps, because a plot beyond 1 mM may exhibit a hyperbolic dependence.

$$k_{obs} = k_1[S] + k_{-1} \quad (27)$$

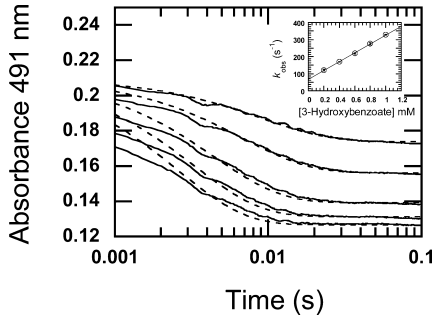

Figure 1. Kinetic traces of the binding of 3-HB to 3HB6H. A solution of the enzyme (31 μM) was mixed with solutions of 3-HB at various concentrations (0.2, 0.4, 0.6, 0.8, and 1 mM, solid lines from top to bottom, respectively). All concentrations quoted are those after mixing. The reactions were performed using the stopped-flow spectrophotometer at 4 °C. The reaction was monitored by following the decrease in absorbance of protein-bound flavin at 491 nm. The traces were fit to a single-exponential phase. The dotted lines show the kinetic traces from simulations using a model of single-step binding according to Scheme 3 and the following parameters: $k_1 = 4 \times 10^5$ M^{-1} s^{-1}, $k_{-1} = 64$ s^{-1}, ε_{491} of $E_{ox} = 6730$ M^{-1} cm^{-1}, and ε_{491} of the E_{ox}·S complex = 3510 M^{-1} cm^{-1}. An empty circle line shows a plot of the observed rate constants obtained from experiments, 122 ± 5, 170 ± 2, 219 ± 3, 276 ± 6, and 328 ± 3 s^{-1} (from low to high 3-HB concentrations as described above), vs 3-HB concentration.

Scheme 3. One-Step Binding Process

$$E_{ox} + S \underset{k_{-1}}{\overset{k_1}{\rightleftharpoons}} E_{ox}{:}S$$

A slope of the plot [(2.6 ± 0.03) × 10^5 M^{-1} s^{-1}] is equivalent to a bimolecular rate constant (k_1) or k_{on}, while the intercept (65 ± 3 s^{-1}) is equivalent to k_{-1} or k_{off} of binding (Table 1).

In addition to the determination of observed rate constants from the kinetic traces, simulations using a one-step binding model according to Scheme 3 were conducted. Using a bimolecular rate constant (k_1^{sim}) of 4 × 10^5 M^{-1} s^{-1} and a reversible rate constant (k_{-1}^{sim}) of 64 s^{-1} resulted in simulated kinetic traces that agree with the experimental data (dotted vs solid lines in Figure 1). At the same 3-HB concentration, apparent rate constants from simulations were higher than the values obtained from the experimental data. This discrepancy reflects uncertainty in the k_1 value because of the loss of the absorption signal during the stopped-flow dead time (0.002 s). The k_{-1}^{sim}/k_1^{sim} ratio (K_d) is 0.16 mM, which is similar to the K_d value of 0.15 ± 0.02 mM that was calculated from the final absorbance change at the reaction time of 2 s when binding was complete (equilibrium) under the same condition. In contrast, the K_d value calculated from the k_{-1}^{obs}/k_1^{obs} ratio is 0.26 mM. These results indicate that the rate constants obtained from simulations are closer to the real values than those obtained from the kinetic traces because of the loss of the absorption signal during the dead time as mentioned above. The K_d value at 4 °C (0.15 ± 0.02 mM) is notably different from the value reported as 0.048 mM at 25 °C.[11]

Kinetics of the Reduction of the Free Enzyme by NADH. A solution of the oxidized enzyme was mixed with various concentrations of NADH under anaerobic conditions using a stopped-flow spectrophotometer. The flavin reduction was monitored at 10 nm intervals from 300 to 600 nm. The data monitored at all wavelengths showed similar kinetics. No

dx.doi.org/10.1021/bi201823c | Biochemistry 2012, 51, 4309−4321

Table 1. Rate Constants Obtained from Kinetic Analysis and Simulations of the Reductive Half-Reactions of 3HB6H in the Presence and Absence of 3-HB

rate constants				extinction coefficients (M^{-1} cm^{-1})[a]	
observed rate constants and equilibrium constants measured from experiments	calculated apparent rate constants from simulations	individual rate constants from simulations[a]	chemical species[a]	452 nm	590 nm
$k_1 = (2.6 \pm 0.03) \times 10^5$ M^{-1} s^{-1}	–	$k_1 = 4 \times 10^5$ M^{-1} s^{-1}	E_{ox}	11300	33
$k_{-1} = 65 \pm 3$ s^{-1}	–	$k_{-1} = 64$ s^{-1}	E_{ox}·S	11200	42
$k_2 = 43 \pm 2$ M^{-1} s^{-1}	–	–	E_{ox}*·S·NADH	10750	280
$K_{d(NADH)} = 1.62 \pm 0.4$ mM	$K_{d(NADH)} = 1.73$ mM	$k_3 = 4.4 \times 10^6$ M^{-1} s^{-1}	E_{ox}·S·NADH	10900	1430
$k_{obs1(app)} = 377 \pm 8$ s^{-1}	$k_{app1(app)} = 354$ s^{-1}[b]	$k_{-3} = 7600$ s^{-1}	E_{red}·S	1460	30
$k_{obs2(app)} = 48 \pm 2$ s^{-1}	$k_{app2(app)} = 49$ s^{-1}[c]	$k_4 = 340$ s^{-1}	–	–	–
–	–	$k_{-4} = 12$ s^{-1}	–	–	–
–	–	$k_5 = 51$ s^{-1}	–	–	–

[a]Rate constants, chemical species, and extinction coefficients from simulations were according to Scheme 5. [b]Apparent rate constant calculated from eq 29. [c]Apparent rate constant calculated from eq 32.

measurable charge transfer with an absorption change in the range of 500–600 nm was detected, indicating that there was no charge-transfer complex, or we possibly observed the linear portion of a hyperbolic dependence. Maximal absorbance changes were observed at 452 nm (Figure 2A), and kinetic traces at this wavelength were used for data analysis. Kinetic traces monitored at 452 nm showed biphasic kinetics (Figure 2A). At the highest NADH concentration of 10 mM (Figure 2A), the first phase (0.002–10 s) showed a decrease in absorbance at 452 nm (~94% of the total amplitude change) according to a rate constant of 0.41 ± 0.01 s^{-1}. The second slower phase was not dependent on NADH concentration and showed a small decrease in absorbance with a rate constant of ~0.05 s^{-1}. This second reduction phase (5–6% of the total amplitude) was observed only at NADH concentrations of ≥0.6 mM because at a low NADH concentration of 0.3 mM, this phase could not be distinguished from the first reduction phase (Figure 2A). The second phase might be due to heterogeneity of the enzyme or reduction of free FAD. The observed rate constants of the first phase are linearly dependent on NADH concentration (Figure 2B) without a significant intercept value. These results suggest that the reduction mechanism of the free enzyme can be described as an irreversible one-step reduction according to Scheme 4. A slope of the plot indicates a bimolecular rate constant (k_2) of 43 ± 2 M^{-1} s^{-1} (Table 1).

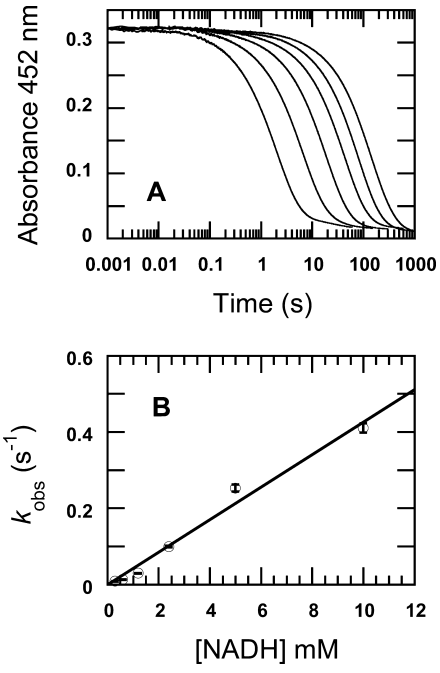

Figure 2. Kinetics of the reduction of free 3HB6H by NADH. A solution of 3HB6H (30 μM) was mixed with solutions of NADH at concentrations of 0.3, 0.6, 1.2, 2.4, 5, and 10 mM (traces from right to left, respectively) under anaerobic conditions using the stopped-flow spectrophotometer at 4 °C. All concentrations quoted are those after mixing. The kinetic traces were fit to two exponential phases. The first exponential phase was flavin reduction with a large absorbance decrease at 452 nm (A). The second exponential phase was a small decrease in absorbance at the same wavelength and is not dependent on NADH concentration. The k_{obs} values of the flavin reduction phase were plotted vs NADH concentration (B). The k_{obs} values according to low to high NADH concentrations as described above are (0.8 ± 0.1) × 10^{-2}, (0.13 ± 0.01) × 10^{-1}, (0.30 ± 0.01) × 10^{-1}, 0.10 ± 0.02, 0.25 ± 0.01, and 0.41 ± 0.01 s^{-1}. A vertical line at each data point indicates a standard deviation of the measurement.

Scheme 4. Reductive Half-Reaction of 3HB6H in the Absence of the Aromatic Substrate

$$E_{ox} + NADH \xrightarrow{k_2} E_{red} + NAD^+$$

Kinetics of Reduction of the 3HB6H·3-HB Complex by NADH. A solution of the oxidized enzyme (28 μM) and 3-HB was mixed with the same buffer containing 3-HB and various NADH concentrations using a stopped-flow spectrophotometer under anaerobic conditions. Flavin reduction was monitored using a diode array detector at wavelength intervals from 300 to 800 nm. The observed charge-transfer intermediate spectrum was observed at wavelength intervals of 500–700 nm (inset of Figure 3B). We observed two dominant spectral changes: a maximal absorbance change due to flavin reduction at 452 nm and an absorbance change at 590 nm due to formation and decay of a charge-transfer complex. Therefore, kinetic traces at both 452 and 590 nm were used for data analysis (Figure 3).

Flavin reduction of the enzyme–substrate complex by NADH resulted in triphasic kinetics, and all wavelengths gave similar observed rate constants. At the highest NADH concentration of 12 mM, the first phase (0.002–0.006 s) was an increase in absorbance at 590 nm (Figure 3B, top trace),

dx.doi.org/10.1021/bi201823c | Biochemistry 2012, 51, 4309–4321

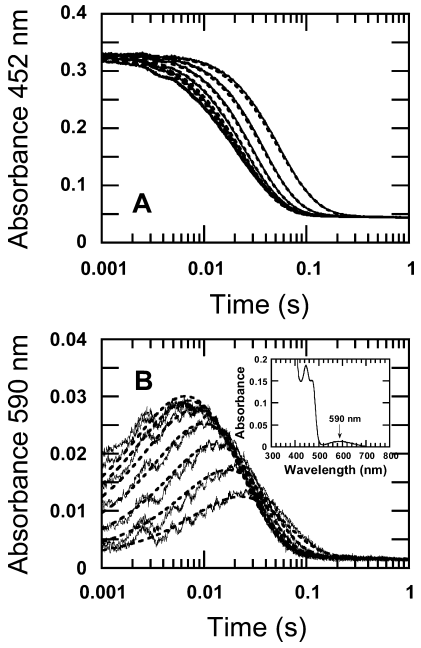

Figure 3. Kinetic traces of the reduction of the 3HB6H·3-HB complex by NADH. A solution of the enzyme (28 μM) and 3-HB (1 mM) was mixed with solutions of 3-HB (10 mM) containing NADH concentrations of 0.2, 0.4, 0.8, 1.6, 3.2, 6.4, and 12 mM (from right to left, respectively). All concentrations quoted are those after mixing. The reactions were performed under anaerobic conditions using the stopped-flow spectrophotometer at 4 °C. The traces were fit to three exponentials. The first exponential phase was a large absorbance increase at 590 nm (with a small absorbance change at 452 nm). The second phase was flavin reduction with a large absorbance decrease at 452 (A) and 590 (B) nm. The third exponential phase was a small decrease in absorbance at 452 nm. The dotted lines represent simulations based on the model presented in Scheme 5 with kinetic parameters listed in Table 1. The inset in panel B shows the observed charge-transfer spectrum obtained from diode array detection at 0.006 s. The arrow indicates the absorbance peak at 590 nm.

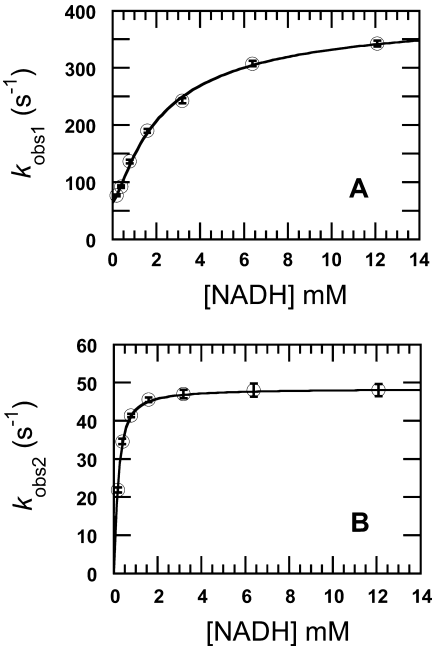

Figure 4. Plot of the observed rate constants (k_{obs}) from the kinetic traces in Figure 3 vs NADH concentration (0.2, 0.4, 0.8, 1.6, 3.2, 6.4, and 12 mM). (A) The observed rate constants (k_{obs1}) were analyzed from the traces of the absorbance change at 590 nm in Figure 3B. The k_{obs1} values of the first phase at low and high NADH concentrations are 76 ± 2, 92 ± 2, 136 ± 3, 190 ± 3, 242 ± 5, 307 ± 5, and 342 ± 5 s^{-1}. The plot of k_{obs1} vs NADH concentration was hyperbolically dependent on NADH concentrations and was analyzed according to eq 28. (B) Observed rate constants of the second phase (k_{obs2}) from the traces of the absorbance changes at 452 and 590 nm (Figure 3). The k_{obs2} values at low to high NADH concentrations are 22 ± 1, 34 ± 1, 41 ± 1, 46 ± 1, 47 ± 1, 48 ± 2, and 48 ± 2 s^{-1}. The plot of k_{obs2} vs NADH concentration was hyperbolically dependent on NADH concentration and analyzed according to eq 31. A vertical line at each data point indicates a standard deviation of the measurement.

whereas the absorbance at 452 nm showed only a small decrease, indicating that the enzyme was mostly in the oxidized form during this phase. The second phase (0.006–0.08 s) showed a decrease in absorbance at 590 nm (Figure 3B), which was synchronized with a large amplitude decrease at 452 nm (Figure 3A). This phase reflects the reduction of the flavin cofactor. The third phase was a small decrease in absorbance at 452 nm (~1.72% of the amplitude of the total change), and a rate constant of 1.82 ± 0.02 s^{-1} was observed over all NADH concentrations.

The observed rate constants (k_{obs1}) of the first phase determined from kinetic traces at 590 nm showed a hyperbolic dependence on NADH concentration (Figure 4A). At high substrate concentrations, the observed rate constants approached a limiting value of 377 ± 8 s^{-1} (Table 1) with an intercept value of 68 ± 3 s^{-1} (Figure 4A). The NADH concentration that gives a half-saturation value of the plot (equivalent to the K_d for binding of NADH to the 3HB6H·3-HB complex) is 1.62 ± 0.4 mM (Table 1 and Figure 4A). Observed rate constants of the second phase (k_{obs2}) analyzed from the kinetic traces monitored at 452 nm also showed a hyperbolic dependence on NADH concentration (Figure 4B) and approached the limiting value of 48 ± 2 s^{-1} (Table 1 and Figure 4B).

Results in Figure 4 are best described using a three-step reduction model shown in Scheme 5. The first step is a rapid binding of NADH to the oxidized enzyme–substrate complex to form the oxidized enzyme·3-HB·NADH complex (E_{ox}*·S·NADH) (Scheme 5). The second step is the

Scheme 5. Reductive Half-Reaction of the 3HB6H·3-HB Complex

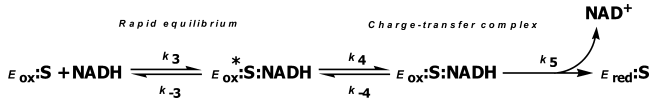

isomerization to form the oxidized enzyme–substrate–NADH charge-transfer complex (E_{ox}·S·NADH), which has maximal absorption around 590 nm. The third step is the decay of the charge-transfer complex due to flavin reduction (Scheme 5), while the last step with a rate constant of 1.82 ± 0.02 s^{-1} (small amplitude change of ~1.72% of the total absorbance change at 452 nm) may be due to heterogeneity of the enzyme or reduction of free FAD.

Simulations according to the model described in Scheme 5 generated data that agree well with the experimental data (Figure 3, solid vs dashed lines). Observed rate constants from the experimental data and apparent rate constants from the

dx.doi.org/10.1021/bi201823c | Biochemistry 2012, 51, 4309–4321

simulations are compared in Table 1. The K_d (k_{-3}/k_3) for the initial binding of NADH to the oxidized enzyme based on simulations (Table 1) was 1.73 mM, which agrees well with the K_d derived from kinetic constants [1.62 ± 0.4 mM (Figure 4A)]. All kinetic constants derived from the experimental data and simulations agree very well, validating the model and kinetic parameters shown in Scheme 5.

The plot of the observed rate constants of the first phase (Figure 4A) was analyzed according to eqs 28 and 29 (derivation in Experimental Procedures). The observed rate constant from the experimental data at the saturating concentration of NADH was determined to be 377 ± 8 s^{-1} from the plot (Figure 4A) and can be described as in eq 28. On the basis of kinetic constants obtained from simulations (Table 1) and eq 29, the apparent rate constant of the first phase, $k_{app1(app)}$, at the saturating concentration of NADH was calculated as 354 s^{-1}, which agrees well with the experimental data.

$$k_{obs1} = \frac{1}{2}\left(\frac{k_4[B]}{K_d + [B]} + k_{-4} + k_5\right) + \left[\frac{1}{4}\left(\frac{k_4[B]}{K_d + [B]} + k_{-4} + k_5\right)^2 - \frac{k_4k_5[B]}{K_d + [B]}\right]^{1/2} \quad (28)$$

$$k_{obs1(saturation)} = \frac{1}{2}(k_4 + k_{-4} + k_5) + \sqrt{\frac{1}{4}(k_4 + k_{-4} + k_5)^2 - k_4k_5} \quad (29)$$

The intercept of the plot of k_{obs1} versus NADH concentration can be described as in eq 30, and the value from the experimental data was determined to be 68 ± 3 s^{-1} (Figure 4A).

$$\text{intercept} = k_{-4} + k_5 \quad (30)$$

Using the rate constants from simulations (Table 1), the value of $k_{-4} + k_5$ was calculated as 63 s^{-1}, which agrees well with the experimental value (68 ± 3 s^{-1}). It should be mentioned that a large uncertainty in the intercept value was due to the limitation in the measurement of k_{obs1}. At NADH concentrations of ≥ 6.4 mM, k_{obs1} could not be measured accurately because a large part of charge-transfer intermediate formation occurred during the dead time (Figure 3B). A plot of observed rate constants of the second phase (Figure 4B) versus NADH concentrations was analyzed according to eq 31 (derivation in Experimental Procedures). The observed rate constant of the second phase (k_{obs2}) at the saturating concentration of NADH can be described as in eq 32 and was measured as 48 ± 2 s^{-1} (Figure 4B). The apparent k_{obs2} at the saturating concentration of NADH based on rate constants from the simulations (Table 1) was calculated as 49 s^{-1}, which agrees well with the experimental data (Table 1).

$$k_{obs2} = \frac{1}{2}\left(\frac{k_4[B]}{K_d + [B]} + k_{-4} + k_5\right) - \left[\frac{1}{4}\left(\frac{k_4[B]}{K_d + [B]} + k_{-4} + k_5\right)^2 - \frac{k_4k_5[B]}{K_d + [B]}\right]^{1/2} \quad (31)$$

$$k_{obs2(app)} = \frac{1}{2}(k_4 + k_{-4} + k_5) - \sqrt{\frac{1}{4}(k_4 + k_{-4} + k_5)^2 - k_4k_5} \quad (32)$$

Therefore, all the comparisons listed in Table 1 indicate very good agreement between the calculated and observed values, validating the kinetic model described in Scheme 5.

Order of Substrate Binding. Rate constants in Table 1 suggest that with the saturating concentrations of NADH (10 mM) and 3-HB (10 mM) used, the oxidized enzyme likely binds to 3-HB faster than to NADH. We then conducted experiments to investigate the order of binding of 3-HB and NADH to the oxidized free enzyme. A solution of 26 μM free oxidized enzyme was mixed with a solution containing 10 mM NADH and 10 mM 3-HB in the stopped-flow spectrophotometer under anaerobic conditions. All concentrations represent those after mixing. The reaction was monitored at 590 and 452 nm. The reaction showed three-phase kinetics similar to the reduction of the enzyme·3-HB complex. The observed rate constants of the first phase (0.002−0.006 s) resulted from formation of the charge-transfer complex at 590 nm approaching the limiting value of 366 ± 10 s^{-1}. Observed rate constants of the second phase (0.006−0.08 s) associated with enzyme reduction were determined from the large amplitude change at 452 nm and approached the limiting value of 51 ± 1 s^{-1} (solid trace, Figure 5). The third phase showed a small amplitude change and was consistent with a rate constant of ~1.82 s^{-1}. As a reference, a solution of the oxidized enzyme (26 μM) premixed with 10 mM 3-HB was mixed with 10 mM NADH and 10 mM 3-HB in the same buffer using the stopped-flow spectrophotometer (filled circle line, Figure 5). The observed rate constant associated with the flavin reduction phase (0.006−0.08 s) for this reaction was 52 ± 1 s^{-1}. The dotted trace shows the control reaction that was the reduction of the free enzyme (26 μM) with 10 mM NADH (Figure 5). The observed rate constant for flavin reduction of the free enzyme at 10 mM NADH was 0.37 ± 0.02 s^{-1}, which is similar to the observed rate constant obtained from an experiment in Figure 2 at a similar NADH concentration. Therefore, the reduction of the free enzyme by NADH (dotted line) is different from that when a solution of NADH and 3-HB was

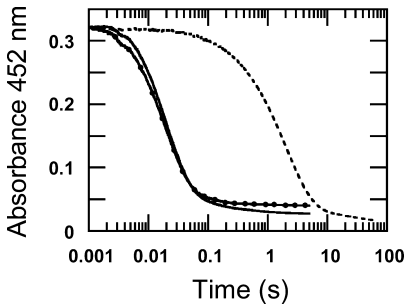

Figure 5. Rapid binding of 3-HB to the oxidized enzyme in the presence of NADH. The solid line was obtained by mixing a solution of the free enzyme (26 μM) with a solution of 10 mM NADH and 1 mM 3-HB, while the filled circle line was obtained by mixing a solution of the enzyme·3-HB complex (26 μM enzyme and 10 mM 3-HB) with 10 mM NADH and 10 mM 3-HB. The dotted line was obtained by mixing a solution of the free enzyme (26 μM) with 10 mM NADH. All concentrations were after mixing.

mixed with the enzyme solution (filled circle line). These results suggest that the order of binding of the substrate for 3HB6H is sequential and the enzyme does not require pre-equilibration with a substrate to attain a stimulatory effect.

Kinetics of the Reduction of the Enzyme–Product Complex by NADH. Single-component flavoprotein hydroxylases are characterized by narrow substrate specificities, although some substrate analogues can act as effectors to stimulate flavin reduction.[12] For 3HB6H, the previous report showed that 2,5-DHB, the product of the reaction, acts as a nonsubstrate effector.[11] The dissociation constant of the enzyme·product complex as determined by static titration experiments (Experimental Procedures) is 0.2 ± 0.01 mM. A solution of the oxidized enzyme (28 μM) in the presence of 2 mM 2,5-DHB (~91% saturation) was mixed with the same concentration of 2,5-DHB with various NADH concentrations using a stopped-flow spectrophotometer under anaerobic conditions. The reactions were performed under the same conditions that were used for the reduction of the enzyme·3-HB complex. The flavin reduction was monitored using a diode array detector at wavelength intervals from 300 to 800 nm. The observed charge-transfer intermediate spectrum was observed at wavelength intervals of 500–700 nm (inset of Figure 6B). The maximal absorbance change due to flavin reduction was observed at 452 nm, while formation of the charge-transfer complex could be clearly observed at 540 nm. Kinetic traces at both 452 and 540 nm were used for data analysis (Figure 6). The flavin reduction observed at 452 nm resulted in four-phase kinetics. At the highest concentration of NADH (12.8 mM), the first phase (0.002–0.02 s) corresponds to an increase in absorbance at 540 nm due to formation of a charge-transfer complex and almost no change in the absorbance at 452 nm, indicating that enzyme was still in the oxidized form during this phase (Figure 6). The kinetic analysis showed the rate constant for formation of a charge-transfer complex of 72 ± 2 s^{-1}, which was independent of NADH concentration. The second phase (0.02–0.2 s) was a large decrease in absorbance at 452 and 540 nm, consistent with a decay of the charge-transfer complex (Figure 6). The observed rate constants of the second phase were hyperbolically dependent on NADH concentration, with an apparent K_d of 4.2 ± 0.4 mM, and approached a limiting value of 45 ± 2 s^{-1} (Figure 7). The third (0.2–0.42 s) and fourth (0.42 until >10 s) phases were small decreases in absorbance at 452 nm with amplitude changes of 12.4 and 3%, respectively, and rate constants of 6.2 ± 0.40 and ~0.54 ± 0.05 s^{-1}, respectively. Neither phase was dependent on NADH concentration.

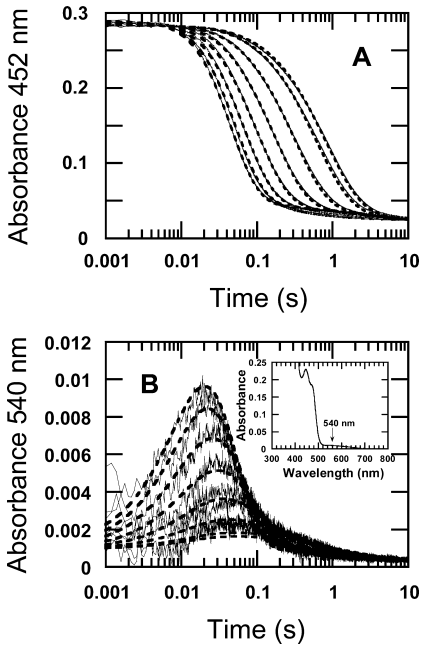

Figure 6. Kinetic traces of the reduction of 3HB6H in a complex with 2,5-DHB. A solution of the enzyme (27 μM) and 2,5-DHB (10 mM) was mixed with solutions of 2,5-DHB (10 mM) containing NADH concentrations of 0.1, 0.2, 0.4, 0.8, 1.6, 3.2, 6.4, and 12.8 mM (from right to left, respectively) under anaerobic conditions using the stopped-flow spectrophotometer at 4 °C. All concentrations quoted are those after mixing. The reaction was fit to three exponentials. The first exponential phase was a large absorbance increase at 540 nm (with a small absorbance change at 452 nm). The second phase was flavin reduction with a large absorbance decrease at 452 and 540 nm. The third exponential phase was a small decrease in absorbance at 452 nm. The dotted lines represent simulations based on the model presented in Scheme 6 with kinetic parameters listed in Table 1. The inset in panel B shows the observed charge-transfer spectrum obtained from diode array detection at 0.02 s. The arrow indicates the absorbance peak at 540 nm.

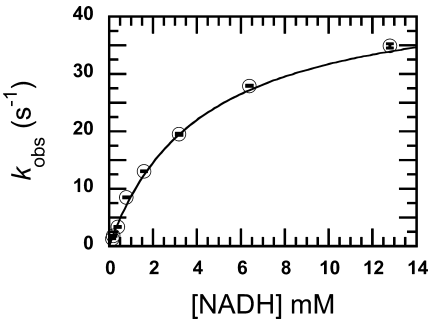

Figure 7. Plot of the observed rate constant (k_{obs}) of flavin reduction (second phase) from the kinetic traces in Figure 6A vs NADH concentration (0.1, 0.2, 0.4, 0.8, 1.6, 3.2, 6.4, and 12.8 mM). The k_{obs2} values at low to high NADH concentrations are 1.2 ± 0.1, 1.8 ± 0.1, 3.3 ± 0.1, 8.4 ± 0.1, 13.0 ± 0.1, 19.0 ± 0.2, 28.0 ± 0.1, and 35.0 ± 0.4 s^{-1}, respectively. The plot of k_{obs2} vs NADH concentration was hyperbolically dependent on NADH concentration and analyzed according to eq 32. A vertical line at each data point indicates a standard deviation of the measurement.

Results in Figures 6 and 7 are best described according to a three-step model shown in Scheme 6. The first step is a rapid binding of NADH to the oxidized enzyme to form the E^*_{ox}·P·NADH oxidized ternary complex (Scheme 6). The second step is the isomerization to form the E_{ox}·P·NADH complex, which is a charge-transfer species that is converted to the reduced enzyme (step 3). This result is consistent with the kinetics at 452 nm in which the enzyme is in the oxidized form during the formation of the charge-transfer species. This interpretation was also confirmed by an independent experi-

Scheme 6. Reductive Half-Reaction of the 3HB6H·2,5-DHB Complex

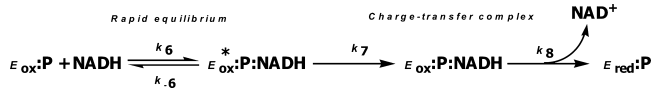

dx.doi.org/10.1021/bi201823c | Biochemistry 2012, 51, 4309–4321

Table 2. Rate Constants Obtained from Kinetic Analysis and Simulations of the Reduction of the 3HB6H·2,5-DHB Complex

rate constants				extinction coefficients (M^{-1} cm^{-1})[a]	
observed rate constants and equilibrium constants measured from experiments	calculated apparent rate constants from simulations	individual rate constants from simulations[a]	chemical species[a]	452 nm	540 nm
–	–	k_6 = 6.5 × 10^5 M^{-1} s^{-1}	E_{ox}	11000	26
–	–	k_{-6} = 2700 s^{-1}	E_{ox}·P	10400	26
k_7 = 46 ± 1.4 s^{-1}	–	k_7 = 39 s^{-1}	E_{ox}·P*·NADH	10700	34
k_8 = 72 ± 2 s^{-1}	–	k_8 = 74 s^{-1}	E_{ox}·P·NADH	10700	1500
$K_{d(NADH)}$ = 4.2 ± 0.4 mM	$K_{d(NADH)}$ = 4.2 mM		E_{red}·P	870	12
k_{obs} = 45 ± 2 s^{-1}[b]	k_{obs} = 39 s^{-1}[c]				

[a]Rate constants, chemical species, and extinction coefficients from simulations were according to Scheme 6. [b]Rate constant obtained from the saturating value of the plot in Figure 7. [c]Rate constant calculated according to eq 34 and parameters in the third column.

ment in which a solution of the reduced enzyme (27 μM) and 2 mM 2,5-DHB was mixed with NAD^+ at concentrations of 0.03, 0.1, 0.25, 0.5, and 9.5 mM using a stopped-flow spectrophotometer. The results showed no absorbance change at 540 nm (data not shown). Therefore, the charge-transfer species must be due to formation of the oxidized enzyme·P·NADH complex.

The observed rate constants for formation of the charge-transfer complex (at 540 nm) were independent of NADH concentration at 72 ± 2 s^{-1}, while the rate constants for decay of the charge-transfer complex were dependent on NADH concentration. These data can be explained according to a rate-switching model[31] in which a rate constant for the decay step (k_8) of the charge-transfer species (E_{ox}·P·NADH) is greater than that of the preceding isomerization step (k_7) ($k_8 > k_7$). Therefore, the intermediate formed with a rate constant of k_8 and decayed with a rate constant of k_7. It suggests that the observed rate constant of 72 ± 2 s^{-1} for the first phase belongs to the flavin reduction rate constant (k_8), whereas the rate constant for the second phase belongs to the isomerization step (k_7).

Simulations according to the model in Scheme 6 were conducted to identify intrinsic rate constants of individual steps. The simulation results agree well with the experimental data (Figure 6, solid vs dashed lines). Observed rate constants from the experimental data and apparent rate constants calculated from the simulations are listed in Table 2. The K_d (k_{-6}/k_6) for binding of NADH to the oxidized enzyme−product complex based on simulations (Table 2) was calculated as 4.2 mM, which agrees with the K_d value determined from observed rate constants [4.2 ± 0.4 mM (Figure 7)]. The simulations yielded a rate constant for charge-transfer decay (k_8) of 74 s^{-1}, which is similar to the observed rate constant of 72 ± 2 s^{-1} for the first phase detected at 540 nm. A plot of the observed rate constants of the reduction step was analyzed according to eq 33, which describes a three-step reduction model modified from eq 26 (derivation in Experimental Procedures) with the reversible rate constant of the second step (k_{-7}) in Scheme 6 equal to zero.

$$k_{obs} = \frac{1}{2}\left(\frac{k_7[B]}{K_d + [B]} + k_8\right) - \sqrt{\frac{1}{4}\left(\frac{k_7[B]}{K_d + [B]} + k_8\right)^2 - \frac{k_7 k_8[B]}{K_d + [B]}} \quad (33)$$

The observed rate constant for the reduction at a saturating concentration of NADH can be described according to eq 34, and this value was measured as 45 ± 2 s^{-1} (plot in Figure 7). Using eq 34 and data from simulations (Table 2), this value was calculated as 39 s^{-1}, which agrees well with the experimental data.

$$k_{obs} = \frac{1}{2}(k_7 + k_8) - \sqrt{\frac{1}{4}(k_7 + k_8)^2 - k_7 k_8} \quad (34)$$

The observed rate constant of the third phase with a value of 6.2 ± 0.4 s^{-1} and the fourth phase (~3% of the total amplitude change), which is consistent with the observed rate constant of ~0.54 ± 0.05 s^{-1}, may be due to the heterogeneity of the enzyme or reduction of free FAD. Overall, the comparison between the calculated and observed values listed in Table 2 indicates good agreement, validating the kinetic model described in Scheme 6 and the reduction mechanism in the presence of 2,5-DHB being similar to the reduction of the enzyme·3-HB complex.

Determination of Reduction Potentials of 3HB6H and the 3HB6H·3-HB Complex. The reduction potentials of the free enzyme and the enzyme·3-HB complex were measured using Massey's method (Experimental Procedures) with indigo disulfonate as the reference dye. Spectra obtained during the reduction (Figure 8A) indicated that both the enzyme and dye were reduced by the xanthine/xanthine oxidase system via a two-electron reduction process without stabilization of any flavin semiquinone species. Absorbances at 458 and 610 nm were used to calculate the concentrations of the oxidized enzyme and dye as described in Experimental Procedures. The midpoint potentials (E^0_m) calculated from the plots of $\log(E_{red}/E_{ox})$ and $\log(D_{red}/D_{ox})$ are −179 ± 1 mV for the enzyme·3-HB complex (Figure 8B) and −175 ± 2 mV for free 3HB6H. The results indicate that the redox potential of the enzyme-bound flavin is not influenced by the binding of 3-HB to the oxidized enzyme.

DISCUSSION

This report describes the investigation of the reduction mechanism of 3HB6H from *R. jostii* RHA1 using transient kinetics. The results clearly illustrate the important role of the aromatic substrate in stimulating the reduction of the enzyme by NADH. The observed rate constant of flavin reduction at saturating concentrations of 10 mM NADH and 10 mM 3-HB is 51 s^{-1} at 4 °C (Table 1), whereas in the absence of 3-HB, flavin reduction occurs with an observed rate constant of 0.43 s^{-1} (calculated from k_2 in Table 1). Substrate-stimulated flavin reduction by NAD(P)H is commonly observed in reactions of single-component flavoprotein hydroxylases such as *p*-hydrox-

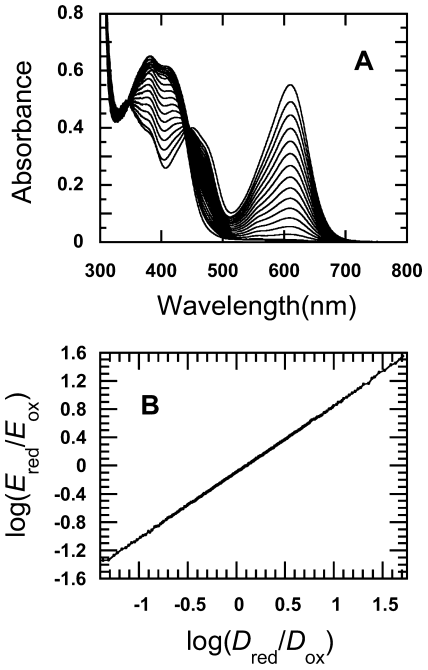

Figure 8. Redox potentials of 3HBH-bound flavin in the presence of 3-HB. The reaction mixture contained 30 μM 3HB6H, 0.5 mM xanthine, 5 μM benzyl viologen, 30 μM indigo trisulfonate, 10 mM 3-HB, and 10 nM xanthine oxidase (side arm). The reaction was performed at 25 °C. The enzyme and dye were slowly reduced under anaerobic conditions using the xanthine/xanthine oxidase reduction system and benzyl viologen as an electron mediator. The top line (450−750 nm) is a spectrum of a mixture of the oxidized enzyme and dye. Other spectra show the progress of the reduction. The reduction of indigo disulfonate was monitored by the absorbance decrease at 610 nm (in which the enzyme had no absorbance), and the reduction of the enzyme was monitored by the decrease in absorbance at 458 nm (isosbestic point of the dye). The inset shows a plot of $\log(E_{red}/E_{ox})$ vs $\log(D_{red}/D_{ox})$. The slope of the plot was 0.94, indicating that two electrons were involved in the reduction of 3HB6H in the presence of 3-HB. The midpoint potential (E^0_m) was calculated as −179 ± 1 mV.

ybenzoate hydroxylase (PHBH),[13,14,32] melilotate hydroxylase,[33] anthranilate hydroxylase,[34] 2-methyl-3-hydroxypyridine-5-carboxylic acid (MHPC) oxygenase (MHPCO),[35,36] 2-hydroxybiphenyl 3-monooxygenase,[37] and kynurenine 3-monooxygenase,[38] or in some reductase components in two-component monooxygenases such as *p*-hydroxyphenylacetate hydroxylase (HPAH) from *Pseudomonas putida*,[39] *Acinetobacter buamannii*,[40,41] and NTA monooxygenase.[42] All these enzyme systems show a slow reduction by NAD(P)H in the absence of substrate or effector. This mechanism prevents wasteful consumption of reduced pyridine nucleotides and toxic hydrogen peroxide production when oxygenation is not possible.[17,18] For 3HB6H, the product of the reaction (2,5-DHB) also acts as an effector to stimulate the flavin reduction with an intrinsic rate constant of 74 s^{-1} (Table 2), which is even faster than the reduction rate constant in the presence of 3-HB. This rate constant cannot be observed at saturating concentrations of 2,5-DHB because it is partially limited by the isomerization rate of the enzyme·2,5-DHB·NADH complex of 45 ± 2 s^{-1}.

The binding of 3-HB to 3HB6H is a single-step binding process forming the enzyme−3-HB complex (E_{ox}·S) with a K_d (k_{-1}/k_1) of 160 μM (Figure 1 and Table 1). The bimolecular rate constant for binding of 3-HB to the oxidized enzyme is 4 × 10^5 M^{-1} s^{-1} (k_{on}) with a reverse rate constant (k_{off}) of 64 s^{-1}. On the other hand, the bimolecular rate constant for NADH reacting with the free oxidized enzyme is 43 ± 2 M^{-1} s^{-1} (k_2 in Table 1). In the presence of both substrates, the binding of 3-HB to the free oxidized enzyme is ∼7400-fold faster than the binding of NADH. Therefore, the substrate binding mechanism for 3HB6H is a sequential type. Under physiological conditions when both NADH and 3-HB are present, enzyme reduction may occur only via the reduction of the 3HB6H−substrate complex as depicted in Figure 5. In this respect, 3HB6H deviates from the reductase component of *p*-hydroxyphenylacetate hydroxylase in which substrate binding to the oxidized enzyme is slow and pre-equilibration of the enzyme and substrate is necessary for formation of the activated enzyme·substrate complex.[41] It should be noted that for the reductase component of *p*-hydroxyphenylacetate 3-hydroxylase, it does not catalyze the oxygenation of *p*-hydroxyphenylacetate but simply uses it as an allosteric effector. Therefore, the rapid binding is not necessary because it needs to bind the effector only once for many turnovers.

The binding of 3-HB to the oxidized enzyme most likely causes some conformational change. Even though the kinetics of reduction by NADH in the presence or absence of 3-HB are different (Figures 2−4), the redox potentials of the free enzyme and enzyme·3-HB complex are similar (−175 ± 2 and −179 ± 1 mV, respectively). This suggests that the stimulation of flavin reduction is not caused by a thermodynamic driving force. A similar observation was made for PHBH.[14] With PHBH, the 10^5-fold stimulation of enzyme reduction upon substrate binding is caused by subtle conformational rearrangements in the active site, including flavin mobility.[14] It is likely that similar conformational rearrangements due to substrate binding are a key factor allowing the reduction stimulation of 3HB6H. In the absence of aromatic ligands, rate constants for 3HB6H reduction are linearly dependent on NADH concentration, indicating that the reduction mechanism is a single-step process without the formation of a Michaelis complex (Figure 2B and Scheme 4). This reaction mechanism is different from that of PHBH in which the free enzyme can form an enzyme−NADH complex prior to flavin reduction.[43] In the presence of 3-HB or 2,5-DHB, observed rate constants for flavin reduction are hyperbolically dependent on NADH concentration (Figures 4B and 7), indicating that an isomerization step occurs after the initial formation of the enzyme·substrate·NADH complex. An isomerization step prior to flavin reduction has also been observed in MHPCO.[35,36]

The isomerization of E^*_{ox}·S·NADH to E_{ox}·S·NADH complexes is accompanied by formation of a charge-transfer complex that has a relatively high extinction coefficient at 590 nm, which is ∼1.43 × 10^3 M^{-1} cm^{-1} (Figure 3B and Table 1). This implies that the isomerization of the oxidized enzyme·3-HB complex causes a closer interaction between oxidized FAD and NADH. Such interaction may be necessary for enhancing the rate of hydride transfer. Previous studies of monomeric sarcosine oxidase with substrate analogues using Raman spectroscopy demonstrated that the regions around the N(5), C(4a), C(10a), and N(1) atoms of the isoalloxazine ring are major interaction sites for formation of the charge-transfer complex.[44] The charge-transfer absorption in the presence of 2,5-DHB has a maximum around 540 nm (Figure 6B), which is hypsochromically shifted compared to the charge-transfer band observed with 3-HB (maximum at 590 nm). This indicates some subtle difference in the electronic interaction between the

dx.doi.org/10.1021/bi201823c | *Biochemistry* 2012, 51, 4309−4321

flavin and nicotinamide rings in the enzyme−substrate and enzyme−product complexes. Whether this interaction between flavin and nicotinamide takes place outside the substrate binding site, as observed with PHBH, is at present unknown. Previous computational interaction studies with medium chain acyl-CoA dehydrogenase showed that the maximal absorption peak for a charge-transfer species depends on the distance between an electron-rich sulfur atom of 3-thiabutanoate ethylthioester and N(5) of the flavin ring. The longer the distance, the longer the wavelength maximum of the charge-transfer band.[45] Therefore, the hypsochromic shift of the maximum of the charge-transfer band in the 2,5-DHB complex compared to the 3-HB complex might be due to a shorter distance between flavin N(5) and C(4) of the reduced nicotinamide.

The reduction mechanism of 3HB6H can be described by Scheme 5, which is a three-step process, and the results can be explained by derivations of kinetic models described in Experimental Procedures. The initial binding of NADH to form an enzyme−substrate complex is a rapid equilibrium, followed by an isomerization step to form the charge-transfer complex with a rate constant of 340 s^{-1} (Figure 4A and Table 1). The flavin reduction then occurs with a rate constant of 51 s^{-1} (Figure 4B and Table 1). A significant intercept value of the hyperbolic plot between the rate constants of the first observed phase and NADH implies that the isomerization step is reversible and the E_{ox}·S·NADH complex can isomerize back to the E^*_{ox}·S·NADH complex (Scheme 5). The derivation of the observed rate constants for the three-step reaction using the method described in Experimental Procedures has also been used to explain a three-step reduction mechanism in pyranose 2-oxidase (P2O).[46] For P2O, substrate binding can be considered a rapid equilibrium, and isomerization is much faster than reduction ($k_1 + k_{-1} \gg k_2 + k_{-2} \gg k_3 + k_{-3}$, where $k_{-3} = 0$). In case of 3HB6H, the binding of NADH to the enzyme·3-HB complex is a rapid equilibrium similar to that of P2O, but the rate constants of the isomerization ($k_3 + k_{-3}$) and reduction ($k_5 + k_{-5}$) steps are comparable ($k_3 + k_{-3} \gg k_4 + k_{-4}$, $k_5 + k_{-5}$, where $k_{-5} = 0$). The value of $k_4 + k_{-4}$ is greater than the value of $k_5 + k_{-5}$ by only 7.6-fold, and the intercept value from the plot of the observed rate constants for isomerization versus NADH (Figure 4A) is the sum $k_{-4} + k_5$ (63 s^{-1}) of the reversible rate constant (k_{-4} = 12 s^{-1}) and reduction rate constant (k_5 = 51 s^{-1}) (eq 30). Therefore, the derivations explained in Experimental Procedures should be useful for interpreting the transient kinetics of many enzymatic systems.

In conclusion, this study has comprehensively elucidated the kinetic mechanism of the reductive half-reaction of 3HB6H from *R. jostii* RHA1. Our results have demonstrated the role of the substrate or product in the stimulation of reduction. A rapid binding of NADH to the 3HB6H·3-HB or 3HB6H·2,5-DHB complex resulted in formation of a charge-transfer complex prior to flavin reduction. The reported results are important for understanding the reaction mechanism of 3HB6H and serve as grounds for an in-depth investigation of the 3HB6H mechanism in the future.

AUTHOR INFORMATION

Corresponding Author

*Department of Biochemistry, Faculty of Dentistry, Chulalongkorn University, Henri Dunant Road, Patumwan, Bangkok 10330, Thailand. Telephone: 662-2188673. Fax: 662-2188670. E-mail: jeerus.s@chula.ac.th.

Funding

This work was supported by The Thailand Research Fund through Grants MRG5380240 (to J.S.) and BRG5480001 (to P.C.), The National Research University Project of CHE and the Ratchadaphiseksomphot Endowment Fund (HR1166I) (to J.S.), the Faculty of Science, Mahidol University (to P.C.), the National Science and Technology Development Agency (to T.W.), and the Integrated Biosynthesis Organic Synthesis (IBOS) project of The Netherlands Organization for Scientific Research (NWO) (to S.M.).

Notes

The authors declare no competing financial interest.

ACKNOWLEDGMENTS

We thank Somchart Maenpuen for critical reading of the manuscript.

ABBREVIATIONS

3-HB, 3-hydroxybenzoate; 3HB6H, 3-hydroxybenzoate 6-hydroxylase; 2,5-DHB, 2,5-dihydroxybenzoate; PHBH, *p*-hydroxybenzoate hydroxylase; P2O, pyranose oxidase; FAD, flavin adenine dinucleotide; k_{obs}, observed rate constant; $k_{cat(app)}$, apparent catalytic constant; E_{red}, reduced form of 3-hydroxybenzoate 6-hydroxylase; E_{ox}, oxidized form of 3-hydroxybenzoate 6-hydroxylase; D_{red}, reduced form of the dye; D_{ox}, oxidized form of the dye; E^0_m, midpoint redox potential.

REFERENCES

(1) Díaz, E. (2004) Bacterial degradation of aromatic pollutants: A paradigm of metabolic versatility. *Int. Microbiol. 7*, 173−180.

(2) Olaniran, A. O., and Igbinosa, E. O. (2011) Chlorophenols and other related derivatives of environmental concern: Properties, distribution and microbial degradation processes. *Chemosphere 83*, 1297−1306.

(3) Lu, X. Y., Zhang, T., and Fang, H. H. (2011) Bacteria-mediated PAH degradation in soil and sediment. *Appl. Microbiol. Biotechnol. 89*, 1357−1371.

(4) Andreoni, V., and Gianfreda, L. (2007) Bioremediation and monitoring of aromatic-polluted habitats. *Appl. Microbiol. Biotechnol. 76*, 287−308.

(5) Harwood, C. S., and Parales, R. E. (1996) The *β*-ketoadipate pathway and the biology of self-identity. *Annu. Rev. Microbiol. 50*, 553−590.

(6) Larkin, M. J., Kulakov, L. A., and Allen, C. C. (2006) Biodegradation by members of the genus *Rhodococcus*: Biochemistry, physiology, and genetic adaptation. *Adv. Appl. Microbiol. 59*, 1−29.

(7) Bell, K. S., Philp, J. C., Aw, D. W., and Christofi, N. (1998) The genus *Rhodococcus*. *J. Appl. Microbiol. 85*, 195−210.

(8) de Carvalho, C. C., and da Fonseca, M. M. (2005) The remarkable *Rhodococcus erythropolis*. *Appl. Microbiol. Biotechnol. 67*, 715−726.

(9) McLeod, M. P., Warren, R. L., Hsiao, W. W., Araki, N., Myhre, M., Fernandes, C., Miyazawa, D., Wong, W., Lillquist, A. L., Wang, D., Dosanjh, M., Hara, H., Petrescu, A., Morin, R. D., Yang, G., Stott, J. M., Schein, J. E., Shin, H., Smailus, D., Siddiqui, A. S., Marra, M. A., Jones, S. J., Holt, R., Brinkman, F. S., Miyauchi, K., Fukuda, M., Davies, J. E., Mohn, W. W., and Eltis, L. D. (2006) The complete genome of *Rhodococcus sp*. RHA1 provides insights into a catabolic powerhouse. *Proc. Natl. Acad. Sci. U.S.A. 103*, 15582−15587.

(10) Liu, T.-T., Xu, Y., Liu, H., Luo, S., Yin, Y. J., Liu, S. J., and Zhou, N. Y. (2011) Functional characterization of a gene cluster involved in gentisate catabolism in *Rhodococcus* sp. strain NCIMB 12038. *Appl. Microbiol. Biotechnol. 90*, 671−678.

(11) Montersino, S., and van Berkel, W. J. (2011) Functional annotation and characterization of 3-hydroxybenzoate 6-hydroxylase from *Rhodococcus jostii* RHA1. *Biochim. Biophys. Acta 1824*, 433−442.
(12) van Berkel, W. J., Kamerbeek, N. M., and Fraaije, M. W. (2006) Flavoprotein monooxygenases, a diverse class of oxidative biocatalysts. *J. Biotechnol. 124*, 670−689.
(13) Entsch, B., and van Berkel, W. J. (1995) Structure and mechanism of *p*-hydroxybenzoate hydroxylase. *FASEB J. 9*, 476−483.
(14) Entsch, B., Cole, L. J., and Ballou, D. P. (2005) Protein dynamics and electrostatics in the function of *p*-hydroxybenzoate hydroxylase. *Arch. Biochem. Biophys. 433*, 297−311.
(15) Palfey, B. A., and McDonald, C. A. (2010) Control of catalysis in flavin-dependent monooxygenases. *Arch. Biochem. Biophys. 493*, 26−36.
(16) Chaiyen, P. (2010) Flavoenzymes catalyzing oxidative aromatic ring-cleavage reactions. *Arch. Biochem. Biophys. 493*, 62−70.
(17) Palfey, B. A., Ballou, D. P., and Massey, V. (1995) Oxygen Activation by Flavins and Pterins. In *Active Oxygen Species in Biochemistry* (Liebman, J. F., and Greenberg, A., Eds.) pp 37−83, Chapman Hall, Glasgow, Scotland.
(18) Ballou, D. P., Entsch, B., and Cole, L. J. (2005) Dynamics involved in catalysis by single-component and two-component flavin-dependent aromatic hydroxylases. *Biochem. Biophys. Res. Commun. 338*, 590−598.
(19) Wang, L. H., Hamzah, R. Y., Yu, Y. M., and Tu, S. C. (1987) *Pseudomonas cepacia* 3-hydroxybenzoate 6-hydroxylase: Induction, purification, and characterization. *Biochemistry 26*, 1099−1104.
(20) Liu, D. Q., Liu, H., Gao, X. L., Leak, D. J., and Zhou, N. Y. (2005) Arg169 is essential for catalytic activity of 3-hydroxybenzoate 6-hydroxylase from *Klebsiella pneumoniae* M5a1. *Microbiol. Res. 160*, 53−59.
(21) Gao, X., Tan, C. L., Yeo, C. C., and Poh, C. L. (2005) Molecular and biochemical characterization of the *xlnD*-encoded 3-hydroxybenzoate 6-hydroxylase involved in the degradation of 2,5-xylenol via the gentisate pathway in *Pseudomonas alcaligenes* NCIMB 9867. *J. Bacteriol. 187*, 7696−7702.
(22) Park, M., Jeon, Y., Jang, H. H., Ro, H. S., Park, W., Madsen, E. L., and Jeon, C. O. (2007) Molecular and biochemical characterization of 3-hydroxybenzoate 6-hydroxylase from *Polaromonas naphthalenivorans* CJ2. *Appl. Environ. Microbiol. 73*, 5146−5152.
(23) Yang, Y.-F., Zhang, J. J., Wang, S. H., and Zhou, N. Y. (2010) Purification and characterization of the *ncgl2923*-encoded 3-hydroxybenzoate 6-hydroxylase from *Corynebacterium glutamicum*. *J. Basic Microbiol. 50*, 599−604.
(24) Yu, Y. M., Wang, L. H., and Tu, S. C. (1987) *Pseudomonas cepacia* 3-hydroxybenzoate 6-hydroxylase: Stereochemistry, isotope effects, and kinetic mechanism. *Biochemistry 26*, 1105−1110.
(25) Rajasekharan, S., Rajasekharan, R., and Vaidyanathan, C. S. (1990) Substrate-mediated purification and characterization of a 3-hydroxybenzoic acid-6-hydroxylase from *Micrococcus*. *Arch. Biochem. Biophys. 278*, 21−25.
(26) Sumathi, S., and Dasgupta, D. (2006) Interaction of 3-hydroxybenzoate-6-hydroxylase with cibacron blue. *J. Enzyme Inhib. Med. Chem. 21*, 47−53.
(27) Massey, V. (1991) A simple method for the determination of redox potentials. In *Flavins and Flavoproteins* (Curti, B., Rochi, S., and Zanetti, G., Eds.) pp 59−66, Water DeGruyter & Co., Berlin.
(28) Clark, W. M. (1960) Compilations of data. In *Oxidation-Reduction Potentials of Organic Systems*, pp 410, Wavery Press, Inc., Baltimore.
(29) Clark, W. M. (1960) The standard hydrogen half-cell and the standardization of oxidation-reduction potentials and pH numbers. In *Oxidation-Reduction Potentials of Organic Systems*, pp 248−272, Wavery Press, Inc., Baltimore.
(30) Bernasconi, C. F. (1976) Relaxation time in common multistep systems. In *Relaxation Kinetics*, pp 40−74, Academic Press, San Diego.
(31) Fersht, A. (1999) Measurement and magnitude of enzymatic rate constants. In *Enzyme Structure and Mechanism*, pp 132−167, W. H. Freeman and Co., NewYork.
(32) Eppink, M. H., Schreuder, H. A., and van Berkel, W. J. (1998) Interdomain binding of NADPH in *p*-hydroxybenzoate hydroxylase as suggested by kinetic, crystallographic and modeling studies of histidine 162 and arginine 269 variants. *J. Biol. Chem. 273*, 21031−21039.
(33) Strickland, S., and Massey, V. (1973) The mechanism of action of the flavoprotein melilotate hydroxylase. *J. Biol. Chem. 248*, 2953−1962.
(34) Powlowski, J., Ballou, D., and Massey, V. (1989) A rapid reaction study of anthranilate hydroxylase. Evidence for a catalytically important conformational change during slow initial turnover with anthranilate. *J. Biol. Chem. 264*, 16008−16016.
(35) Chaiyen, P., Brissette, P., Ballou, D. P., and Massey, V. (1997) Thermodynamics and reduction kinetics properties of 2-methyl-3-hydroxypyridine-5-carboxylic acid oxygenase. *Biochemistry 36*, 2612−2621.
(36) Chaiyen, P., Brissette, P., Ballou, D. P., and Massey, V. (1997) Reaction of 2-methyl-3-hydroxypyridine-5-carboxylic acid (MHPC) oxygenase with N-methyl-5-hydroxynicotinic acid: Studies on the mode of binding, and protonation status of the substrate. *Biochemistry 36*, 13856−13864.
(37) Suske, W. A., van Berkel, W. J., and Kohler, H. P. (1999) Catalytic mechanism of 2-hydroxybiphenyl 3-monooxygenase, a flavoprotein from *Pseudomonas azelaica* HBP1. *J. Biol. Chem. 274*, 33355−33365.
(38) Crozier-Reabe, K. R., Phillips, R. S., and Moran, G. R. (2008) Kynurenine 3-monooxygenase from *Pseudomonas fluorescens*: Substrate-like inhibitors both stimulate flavin reduction and stabilize the flavin-peroxo intermediate yet result in the production of hydrogen peroxide. *Biochemistry 47*, 12420−12433.
(39) Arunachalam, U., Massey, V., and Miller, S. M. (1994) Mechanism of *p*-hydroxyphenylacetate 3-hydroxylase. A two-protein enzyme. *J. Biol. Chem. 269*, 150−155.
(40) Chaiyen, P., Suadee, C., and Wilairat, P. (2001) A novel two-protein component flavoprotein hydroxylase. *Eur. J. Biochem. 268*, 5550−5561.
(41) Sucharitakul, J., Chaiyen, P., Entsch, B., and Ballou, D. P. (2005) The reductase of *p*-hydroxyphenylacetate 3-hydroxylase from *Acinetobacter baumannii* requires *p*-hydroxyphenylacetate for effective catalysis. *Biochemistry 44*, 10434−10442.
(42) Uetz, T., Schneider, R., Snozzi, M., and Egli, T. (1992) Purification and characterization of a two-component monooxygenase that hydroxylates nitrilotriacetate from "Chelatobacter" strain ATCC 29600. *J. Bacteriol. 174*, 1179−1188.
(43) Howell, L. G., Spector, T., and Massey, V. (1972) Purification and properties of *p*-hydroxybenzoate hydroxylase from *Pseudomonas fluorescens*. *J. Biol. Chem. 247*, 4340−4350.
(44) Zheng, Y., Wagner, M. A., Jorns, M. S., and Carey, P. R. (2001) Selective enhancement of ligand and flavin Raman modes in charge-transfer complexes of sarcosine oxidase. *J. Raman Spectrosc. 32*, 79−92.
(45) Tanaka, T., Tamaoki, H., Nishina, Y., Shiga, K., Ohno, T., and Miura, R. (2006) Theoretical study on charge-transfer interaction between acyl-CoA dehydrogenase and 3-thiaacyl-CoA using density functional method. *J. Biochem. 139*, 847−855.
(46) Prongjit, M., Sucharitakul, J., Wongnate, T., Haltrich, D., and Chaiyen, P. (2009) Kinetic mechanism of pyranose 2-oxidase from *Trametes multicolor*. *Biochemistry 48*, 4170−4180.